environments

MDPI

Article

Study on Nutrient Release Characteristics During the Decomposition of *Potamogeton crispus* L. in the Huayang Lakes

Xiaoning Jia [1], Yanhui Yang [1,2], Zhuming Liang [2], Fansheng Meng [2,*], Lingsong Zhang [2], Hao Xue [2] and Na Liu [2]

[1] School of Metallurgy and Environmental Science, Lanzhou University of Technology, Lanzhou 730050, China
[2] Research Center for Environmental Pollution Control Engineering Technology, Chinese Research Academy of Environmental Sciences, Beijing 100020, China; liuna_1231@163.com (N.L.)
* Correspondence: mengfs@craes.org.cn

Abstract

The senescence and decomposition of *Potamogeton crispus* L. are critical drivers of internal nutrient loading and eutrophication in shallow lakes during late spring. Combining field monitoring and laboratory microcosm experiments, we investigated the effects of temperature (20–30 °C) and biomass loading on nutrient release from *P. crispus*, and the underlying microbial mechanisms. Results showed that total phosphorus (TP) release followed an asymptotic exponential model (R^2 = 0.98), with a half-life of only 12.2 d, and 30 °C increased the final TP concentration by 42.1% compared with 20 °C. A biomass loading of 30 g was identified as the critical threshold for water quality deterioration. Nutrient release showed significant asynchrony (TP >> TN ≈ TC), and microbial communities exhibited distinct functional succession under different temperature and biomass conditions. This study provides a scientific basis for targeted management of internal loading in shallow lakes.

Keywords: submerged macrophytes; decomposition; nutrient release; temperature; endogenous pollution

1. Introduction

Submerged macrophytes, serving as the ecological foundation of shallow lake ecosystems, maintain aquatic ecological balance by providing three-dimensional habitats, assimilating nutrients, and suppressing algal competition [1,2]. However, the ecological effects driven by their life cycle rhythms exhibit significant complexity. As a dominant submerged macrophyte in temperate and subtropical lakes, *Potamogeton crispus* L. possesses unique phenological characteristics: winter germination, rapid spring proliferation, and concentrated senescence in late spring. It serves as a crucial vector for biogeochemical cycling within lake ecosystems [3]. During the senescence phase, massive amounts of *P. crispus* litter settle onto the sediment surface. Through microbial decomposition and mineralization, the nitrogen (N), phosphorus (P), and other nutrients previously assimilated in the plant tissues are released back into the water column. This process triggers a surge in internal loading and accelerates the eutrophication of the water body, acting as a primary driver of water quality deterioration in many shallow lakes during late spring and early summer [4,5].

The Middle and Lower Yangtze River Plain is a concentrated region of shallow lakes in China, where *P. crispus* is widely distributed across the majority of these lakes (e.g., Lake Chaohu, Lake Hongze, and Lake Gaoyou). Recent monitoring data indicate that these lakes frequently experience profound water quality fluctuations from April to June: dissolved

Check for updates

Received: 6 March 2026
Revised: 22 April 2026
Accepted: 8 May 2026
Published: 20 May 2026

Copyright: © 2026 by the authors. Licensee MDPI, Basel, Switzerland. This article is an open access article distributed under the terms and conditions of the Creative Commons Attribution (CC BY) license.

oxygen (DO) levels drop below 3 mg/L, total nitrogen (TN) and total phosphorus (TP) concentrations increase by two- to three-fold compared to the growing season, and the permanganate index (COD_{Mn}) rises synchronously [6]. In some areas, these conditions even trigger cyanobacterial blooms [7,8]. This phenomenon coincides closely with the concentrated die-off period of *P. crispus*. Accordingly, by combining long-term field monitoring data with laboratory microcosm experiments, this study systematically investigates the decomposition rates and nutrient release dynamics of *P. crispus* under various combinations of temperature and biomass loading [9]. This study proposes and tests three core hypotheses: (1) Temperature and biomass loading serve as independent primary drivers for the decomposition process of *P. crispus* litter. An increase in either factor will significantly accelerate nutrient release rates and exacerbate aquatic hypoxia. (2) Due to the distinct chemical binding forms and degradation pathways of C,N, and P within plant tissues, their release during decomposition will exhibit significant asynchrony (e.g., the rapid leaching of highly soluble elements outpaces the release of structural elements dependent on enzymatic hydrolysis). (3) The impact of macrophyte litter loading on water quality will exhibit a non-linear response, suggesting the existence of a critical ecological biomass threshold. Once this threshold is exceeded, the nutrient flux released from the decomposing litter will completely overwhelm the self-purification and retention capacities of the water body, leading to an abrupt deterioration in water quality [10]. By validating these hypotheses, this study aims to provide a robust theoretical foundation for the scientific management and targeted control of *P. crispus* communities in shallow lakes.

2. Study Area

The Huayang Lakes (115°58′ E–116°35′ E, 29°52′ N–30°18′ N) are situated in the riparian plain of southwestern Anhui Province on the northern bank of the middle and lower reaches of the Yangtze River. Administratively encompassing parts of Susong, Wangjiang, and Taihu counties in Anqing City, Anhui Province, they constitute a crucial component of the shallow lake groups in the Middle and Lower Yangtze River Plain and serve as a typical representative of the river–lake complex ecosystems in the Yangtze River Basin (the distribution of the study area is shown in Figure 1) [11]. Significantly influenced by the artificial regulation of the Huayang Sluice, the lakes exhibit a unique hydrological rhythm characterized by connection to the river during the flood season and sluice closure during the dry season [12]. This sluice-controlled hydrological regime fundamentally alters natural hydrological processes, hindering the rapid flushing of nutrients and thereby accumulating an abundant material basis for the growth of *P. crispus* [13].

These lakes are classified as typical shallow lakes, with an average water depth of 1.5–2.5 m and a maximum depth not exceeding 4 m. Shallow areas with depths of 1–2 m account for over 80% of the total area, creating highly favorable topographic conditions for the growth of submerged macrophytes such as *P. crispus* [14]. In this shallow-water environment, sufficient light penetrates directly to the lake bottom, satisfying the photosynthetic demands of *P. crispus* and supporting its rapid proliferation to form dominant communities [15]. The shallow depth (1–2 m for over 80% of the area) provides sufficient light for *P. crispus* growth, forming dominant communities that contribute to significant internal nutrient loading during senescence [6].

Based on the analysis of Sentinel-2 Multispectral Instrument (MSI) satellite observation data from 2019 to 2022 (Figure 2) [16], the aquatic vegetation in the Huayang Lakes exhibited a spatial distribution pattern dominated by Lake Huang, with Lake Longgan playing a secondary role. Specifically, the maximum aquatic vegetation area in Lake Huang reached 109.91 km^2, with a vegetation occurrence rate of 18.31%, both of which were significantly higher than those in Lake Longgan. As typical shallow lakes with an average depth

of ≤6 m, the abundant nutrient supply and favorable hydraulic retention times (165.4 to 206.2 days) jointly facilitated the lush growth of dominant species such as *P. crispus*.

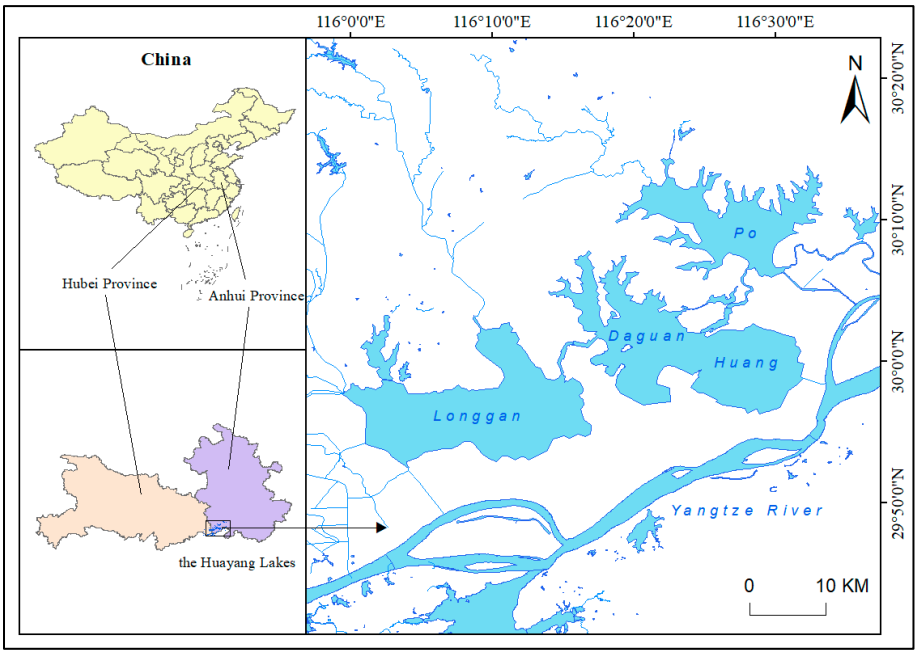


Figure 1. Distribution map of study areas.

This pronounced spatial variation indicates a high degree of spatial heterogeneity in *P. crispus* biomass across the lake group, suggesting that decomposition habitats are profoundly influenced by the dual effects of temperature and substrate loading. This pronounced spatial variation indicates a high degree of spatial heterogeneity in *P. crispus* biomass across the lake group, suggesting that decomposition habitats are profoundly influenced by the dual effects of temperature and substrate loading.

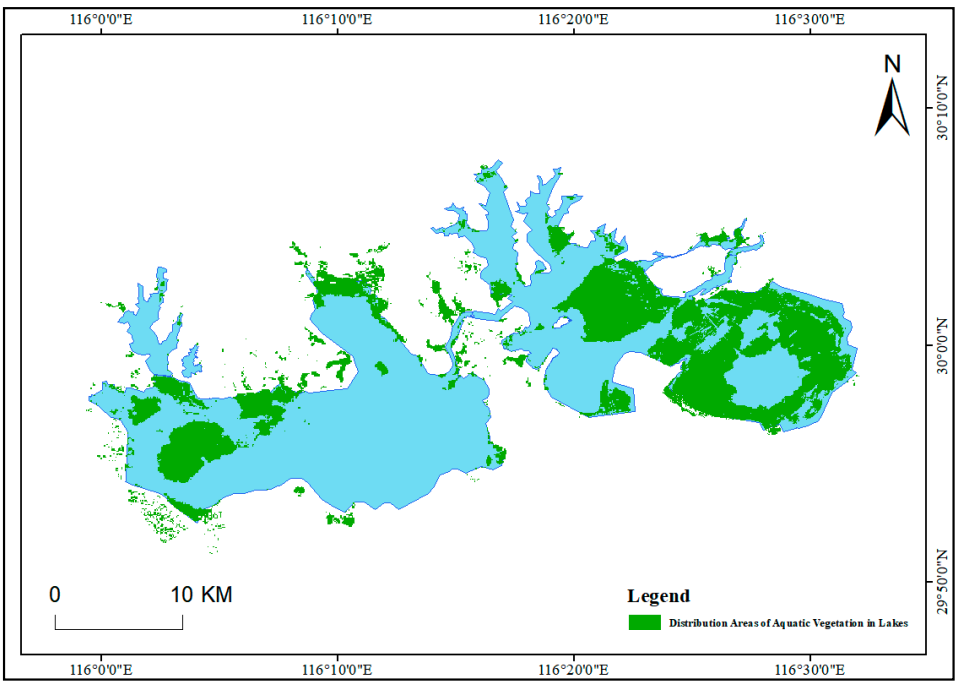


Figure 2. Distribution map of aquatic vegetation in the Huayang Lakes.

3. Methods

3.1. Collection of Long-Term Monitoring Data

The long-term monitoring data for this study were obtained from the National Surface Water Quality Automatic Monitoring Stations (state-controlled stations) situated within the Huayang River Lake Group, ensuring high spatial consistency between the monitoring sites and the study area. The monitoring parameters encompassed water temperature, pH, DO, electrical conductivity, turbidity, COD_{Mn}, NH_4^+-N, TP, TN, chlorophyll-a, and transparency, facilitating real-time tracking of core water quality and hydrological variables. By analyzing the correlations among these indicators, the dynamic evolution of water quality in Lake Daguan, Lake Huang, and Lake Longgan was characterized in depth, focusing on both interannual trends and seasonal variations.

3.2. Collection of Test Samples

The fresh *P. crispus* specimens were thoroughly rinsed with tap and deionized water to remove epiphytic algae and impurities. The cleaned samples were then dried at 75 °C to a constant weight, fragmented into 2–3 cm segments, and homogenized to ensure substrate consistency across experimental groups.

3.3. Experimental Design

To investigate the decomposition patterns under various environmental conditions, a series of microcosm experiments was conducted by controlling different factors. The specific experimental settings are summarized in Table 1. The experiments were carried out from April to July 2025, with three replicates established for each group to ensure data reliability. The experimental design was grounded in the following scientific rationales:

Table 1. Decomposition test setup.

Serial Number	Group	Biomass Loading of *P. crispus*/g	Temperature/°C	Number of Sets
1	K0 (Lake water + sediment)	0	20	3
2	M1 (Lake water + sediment)	20	20	3
3	M2 (Lake water + sediment)	20	25	3
4	M3 (Lake water + sediment)	20	30	3
5	M4 (Lake water + sediment)	30	20	3
6	M5 (Lake water + sediment)	40	20	3
7	K1 (Pure water)	20	20	3
8	K2 (lake water)	20	20	3

Replication Strategy: Each group was tested in triplicate to ensure statistical robustness, allowing for the calculation of standard deviations and the execution of rigorous Two-way ANOVA to detect significance.

Biomass Loading Design: Biomass loading levels (20, 30, 40 g) simulated extreme local accumulation of senescent macrophytes in natural lakes, amplifying nutrient release signals to avoid masking by background sediment fluctuations. It should be clarified that these loading levels do not represent the average biomass density of the entire lake, but rather target the high-density accumulation hotspots (e.g., bays, littoral zones) formed by wind-wave-driven aggregation of senescent macrophytes—zones recognized as key sources of internal eutrophication [17]. For each 5 L reactor (sediment–water interface area = 154 cm^2, calculated as πr^2 where r = 7 cm), the 20 g, 30 g, and 40 g loadings correspond to areal loadings of 129.9 g/m^2, 194.8 g/m^2, and 259.7 g/m^2, respectively. These values are consistent with the local accumulation density (100–300 g/m^2) of senescent *P. crispus* litter

observed in field surveys of the Huayang Lakes, verifying the ecological rationale of the experimental setup.

Disposable 5 L plastic cylinders (Figure 3) were used as reactors, each containing 1 L of in situ sediment and 4 L of filtered lake water. See Table 2 for the experimental setup. After 3 days of equilibration, fragmented *P. crispus* samples were uniformly distributed and allowed to settle freely on the sediment–water interface, simulating natural decomposition. Water samples (100 mL) were collected on days 0, 2, 4, 6, 8, 10, 12, 15, 18, 21, 24, 27, 30, 40, 50, 60, 80, 100, and 120 using a syringe equipped with a 10 cm plastic tube. For the determination of ammonium nitrogen (NH_4^+-N), the collected water was filtered through a 0.45 μm glass fiber filter. Raw (unfiltered) water was used directly for the measurement of TN, TP, and COD_{Mn}. Simultaneously, DO and pH were measured in situ at a depth of 5 cm below the water surface using a portable multi-parameter water quality analyzer. To avoid disturbing the anaerobic microenvironment at the sediment–water interface, any agitation of the water column was strictly prohibited during the measurement and sampling periods. This study adopted a single-factor control design to independently quantify the individual effects of temperature and biomass loading, avoiding the confounding effects of multi-factor interactions. The full factorial combination of high biomass and elevated temperatures will be verified in future in situ mesocosm experiments, as specified in the Section Limitations and Future Prospects.



(**a**) (**b**)

Figure 3. Photographs of the sampling site and simulation experimental setup. (**a**) Field test photographs. (**b**) Simulation experiment photographs.

Table 2. Experimental design for nutrient dynamics during *P. crispus* decomposition.

Serial Number	Group	Biomass Loading of *P. crispus*/g	Temperature/°C	Number of Sets	Sampling Events/d
1	MA	20	20	3	5
2	MB	20	20	3	10
3	MC	20	20	3	15
4	MD	20	20	3	20
5	ME	20	20	3	25
6	MF	20	20	3	30
7	MG	20	20	3	40
8	MH	20	20	3	50
9	MI	20	20	3	60
10	MJ	20	20	3	80
11	MK	20	20	3	100
12	ML	20	20	3	120

To protect the fragile anaerobic microenvironment at the sediment–water interface and prevent sediment resuspension, independent parallel groups (MA–ML) were specifically established for plant residue sampling. These groups were maintained under identical conditions to the main experimental reactors but were used exclusively for sequential biomass retrieval, ensuring that water quality monitoring remained undisturbed by physical sampling.

3.4. Water Quality Testing

a. Water Quality Testing

TN, TP, COD_{Mn}, and NH_4^+-N were determined in accordance with the following national standards of China: "Water Quality -determination of Total Nitrogen-Potassium Persulfate Alkaline digestion and Ultraviolet Spectrophotometric Method" (HJ 636-2012) [18], "Water Quality -determination of Total Phosphorus-Ammonium Molybdate Spectrophotometric Method" (GB 11893-1989) [19], "Water Quality-determination of Permanganate Index" (GB/T 11892-1989) [20], and "Water Quality-determination of Ammonia Nitrogen-Nessler's Reagent Spectrophotometric Method" (HJ 535-2009) [21]. During testing, pH and DO were measured using a YSI ProQuatro multiprobe (YSI, Yellow Springs, OH, USA) with a measurement error of $\pm$0.2 mg/L for DO.

b. Determination of Plant Residues

On days 0, 5, 10, 15, 20, 25, 30, 40, 50, 60, 80, 100, and 120 of the experiment, *Potamogeton crispus* L. residues were collected from each parallel group. After rinsing the surface attachments with deionized water, the residues were dried to a constant weight at 75 °C. The TC and TN contents of the plant residues were determined using an elemental analyzer (Vario EL cube, Elementar, Germany). For TP determination, the plant residues underwent acid digestion and were subsequently analyzed using an inductively coupled plasma optical emission spectrometer (ICP-OES, iCAP 7200, Thermo Fisher Scientific, Waltham, MA, USA).

c. Microbial Community Analysis

At the end of the experiment, overlying water samples were collected from the reactors. Microorganisms were enriched through sterile filtration, after which the bacterial 16S rRNA genes were subjected to high-throughput sequencing by a professional agency to analyze the diversity and composition characteristics of the microbial community.

3.5. Data Analysis

Data plotting and visualization were performed using Origin 2021 software (OriginLab, Northampton, MA, USA), with all data points in the figures expressed as the mean $\pm$ standard deviation (SD). Statistical analyses were conducted using SPSS 26.0 software (IBM, Chicago, IL, USA). For the definition of hypoxia in this study, we adopted the standards proposed by Hrustić and Bobanović-Ćolić (2017) [22]. The water column is considered hypoxic when the dissolved oxygen (DO) concentration is below 2.0 mg/L, and severe hypoxia is noted at lower measurable levels. The term anoxia is strictly reserved for conditions with fundamentally no measurable oxygen. To elucidate the individual and combined effects of temperature and *P. crispus* biomass loading on water quality parameters (e.g., TP and TN), two-way analysis of variance (Two-way ANOVA) was employed to evaluate the significance of the main effects and their interaction effects. A p-value < 0.05 was considered statistically significant.

The Olson index decay model was employed to fit the residual rates of carbon and nitrogen elements in *P. crispus* residues, thereby quantifying decomposition rates [7]. The formula is as follows:

$$y_t = M_0 \times e^{-kt} \quad (1)$$

In the equation: y_t represents the residual amount (or content) of the element in plant residues at time t; M_0 denotes the initial amount; k is the decomposition constant, d^{-1}; a higher value indicates faster release; and t is the decomposition time, d.

An asymptotic exponential decay model was employed to fit the residual rate of phosphorus in *P. crispus* residues [9]. The formula is as follows:

$$y_t = a \times e^{-kt} + b \quad (2)$$

In the equation: y_t represents the elemental content at time t; a denotes the content of the readily decomposable/releasable fraction, which rapidly diminishes over time; b represents the content of the recalcitrant residue/stable fraction, constituting the theoretical limit value (asymptote) of y_t as time approaches infinity; and k is the decomposition constant for the readily decomposable fraction.

Based on the estimated decomposition rate constant (k), the nutrient release half-life ($t_{0.5}$, representing the time required for 50% release) and the 95% release time ($t_{0.95}$) were calculated using the equations $t_{0.5} = \ln(2)/k$ and $t_{0.95} = \ln(20)/k$, respectively.

4. Results and Analysis

4.1. Water Ecological Characteristics of the Huayang Lakes

4.1.1. Interannual Variability Trends

The interannual water quality evolution in the Huayang Lakes from 2020 to 2025 exhibited distinct parameter-specific variations and lake-level differentiation (Table 3). NH_4^+-N concentrations decreased significantly across all three lakes, with Lake Longgan showing the largest reduction (82.5%, Table 3). TP concentrations exhibited divergent trends: Lake Daguan and Lake Huang declined to historical lows in 2025, while Lake Longgan increased by 46.2% (Table 3). Furthermore, TN concentrations in all three lakes peaked in 2024 (e.g., Lake Huang reached a maximum of 1.34 mg/L), while COD_{Mn} in Lake Longgan increased significantly from 2.86 to 5.12 mg/L [23]. Pearson correlation analysis (Figures 4–6) reveals significant positive correlations between TP and TN across the three lakes ($r = 0.44–0.58$, $p < 0.05$; $p < 0.001$ for Lake Daguan and Lake Longgan), suggesting the presence of synergistic external inputs or internal nutrient release [24]. Additionally, a significant negative correlation between COD_{Mn} and NH_4^+-N was identified in Lake Longgan ($r = -0.38$, $p < 0.01$), which may reflect the consumption and transformation of nitrogen during the decomposition of organic substrates [25].

Table 3. Statistical table of interannual data for key water quality parameters of the three lakes, 2020–2025 (mg/L).

Name of the Lake	Year	TP	TN	COD_{Mn}	NH_4^+-N
Lake Longgan	2020	0.052	0.77	4.2	0.06
	2021	0.058	0.89	5.3	0.07
	2022	0.065	0.98	5.6	0.08
	2023	0.071	1.05	5.8	0.09
	2024	0.073	1.15	5.5	0.08
	2025	0.076	1.12	5.4	0.07

Table 3. *Cont.*

Name of the Lake	Year	TP	TN	COD_{Mn}	NH_4^+-N
Lake Daguan	2020	0.032	0.68	3.5	0.04
	2021	0.035	0.72	3.8	0.03
	2022	0.033	0.65	4.1	0.04
	2023	0.031	0.35	4.3	0.05
	2024	0.038	0.86	4.5	0.04
	2025	0.034	0.61	4.2	0.03
Lake Huang	2020	0.036	0.75	3.2	0.05
	2021	0.039	1.19	3.6	0.06
	2022	0.041	0.82	3.9	0.04
	2023	0.037	0.51	4	0.03
	2024	0.046	1.34	4.3	0.05
	2025	0.038	0.78	4.1	0.04

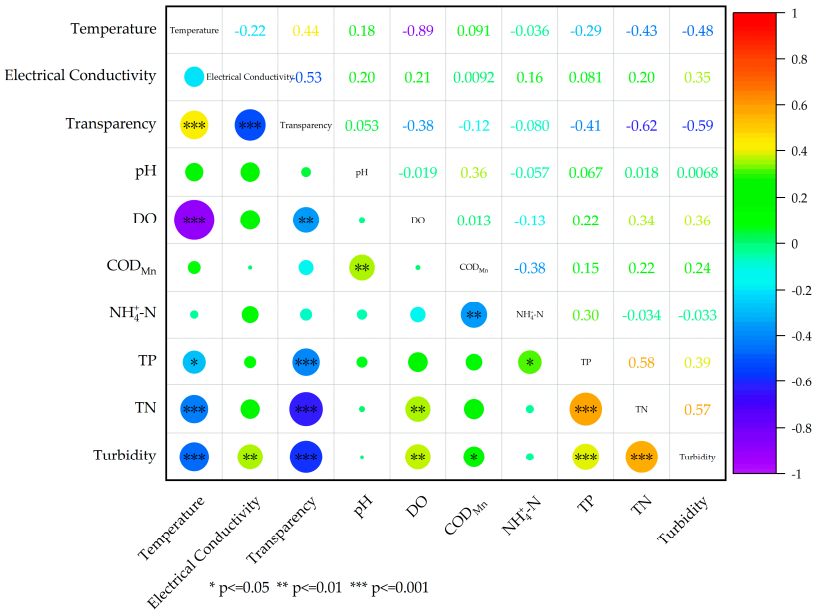


Figure 4. Correlation analysis of water quality at the Lake Longgan monitoring point (2020–2025).

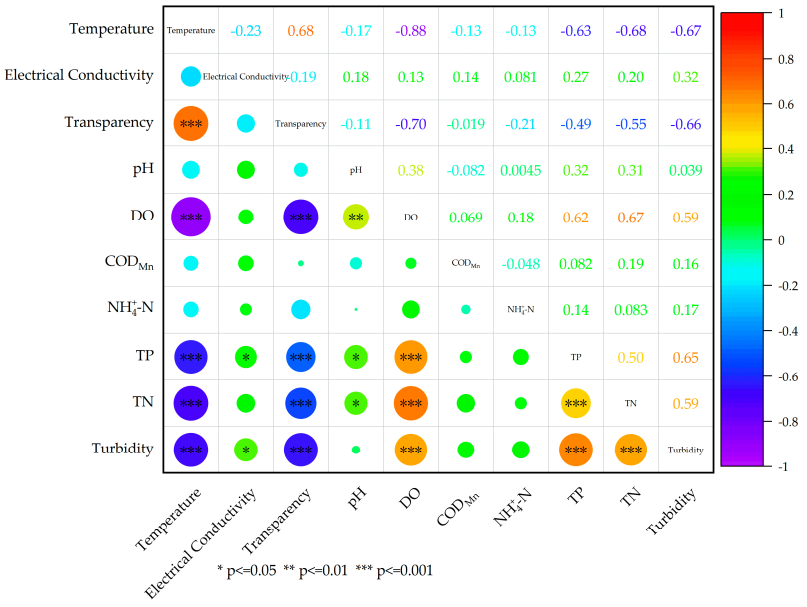


Figure 5. Correlation analysis of water quality at the Lake Daguan monitoring point (2020–2025).

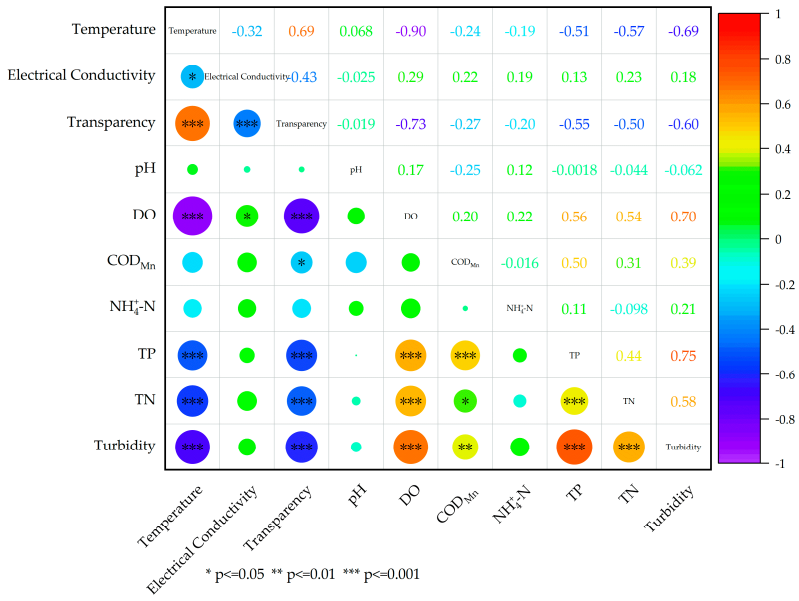


Figure 6. Correlation analysis of water quality at the Lake Huang monitoring point (2020–2025).

4.1.2. Seasonal Variation Trends

Figures 7–9 present boxplots illustrating the seasonal distribution of water quality parameters in the three lakes from 2020 to 2025. Driven by hydrological rhythms and biogeochemical processes, the water quality of the Huayang Lakes exhibited a typical "winter-worse, summer-better" seasonal pattern. Mean TP and TN concentrations across all three lakes were significantly higher in winter and spring than in summer and autumn. For instance, the mean TN in Lake Huang during winter reached as high as 1.14 mg/L, more than triple the summer average (0.33 mg/L); a similar trend was observed for TP in Lake Daguan. These seasonal discrepancies may be attributed to the physical concentration effect during the winter–spring dry season, the temperature-induced inhibition of microbial degradation activity, and the passive accumulation of nutrients resulting from macrophyte litter decomposition. Conversely, the hydraulic dilution effect during the summer high-water period, combined with the biological sink effect facilitated by the vigorous growth of aquatic plants, collectively promoted the improvement of water quality [26]. Notably, Lake Longgan exhibited an anomalous summer peak in NH_4^+-N concentration, with a summer mean of 0.08 mg/L, which was higher than the levels observed in winter and spring. Seasonal fluctuations in COD_{Mn} were relatively stable across the three lakes, with a general trend of slightly higher values in autumn and winter. Specifically, COD_{Mn} in Lake Longgan peaked in autumn (5.2 mg/L), which is likely related to the timing of concentrated macrophyte senescence and the subsequent release of dissolved organic matter into the water column [27].

4.2. Changes in Plant Nutrients

Nutrient release from *P. crispus* residues showed significant asynchrony, with the release rate following the order of TP > TN ≈ TC (Figure 10). TP exhibited the most rapid release (cumulative loss 65.5%) due to physical leaching: cell membrane rupture after plant death triggers rapid diffusion of intracellular water-soluble phosphates into the water column. TN loss (35.7%) involves initial physical leaching of free amino acids and subsequent microbial mineralization-immobilization balance, leading to slow sustained release [28]. TC loss (33.8%) is the slowest, as cellulose and lignin depend on microbial enzymatic hydrolysis, with recalcitrant components converted into humus for long-term carbon sequestration [29].

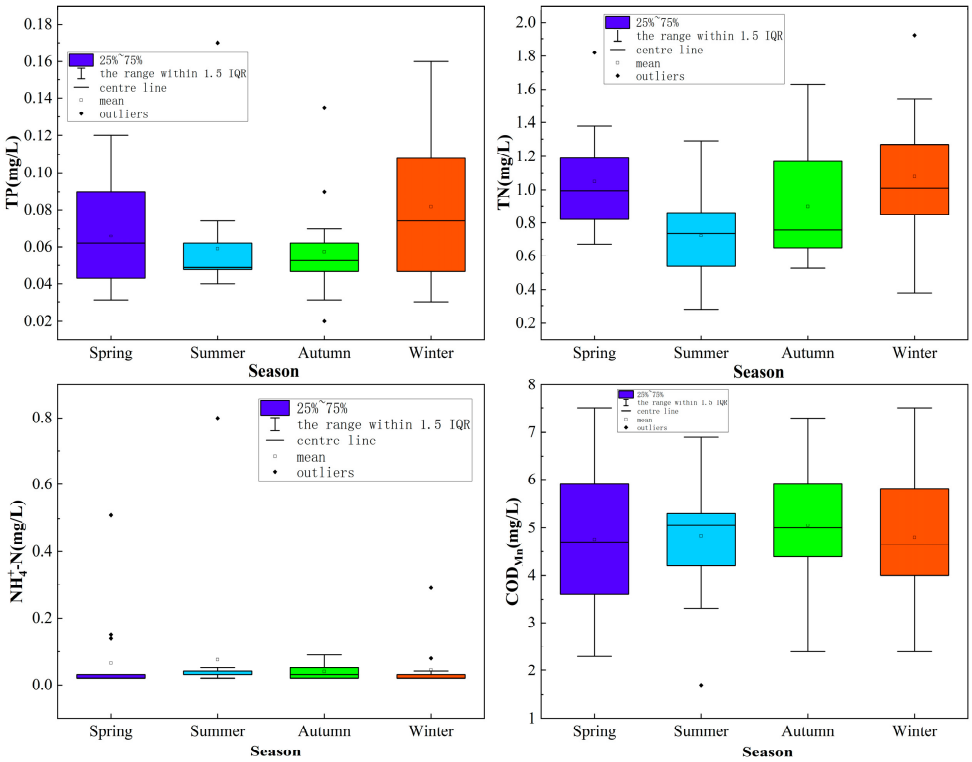


Figure 7. Seasonal variations in water quality indicators in Lake Longgan from 2020 to 2025 (The different colours simply represent different seasons; they have no other significance).

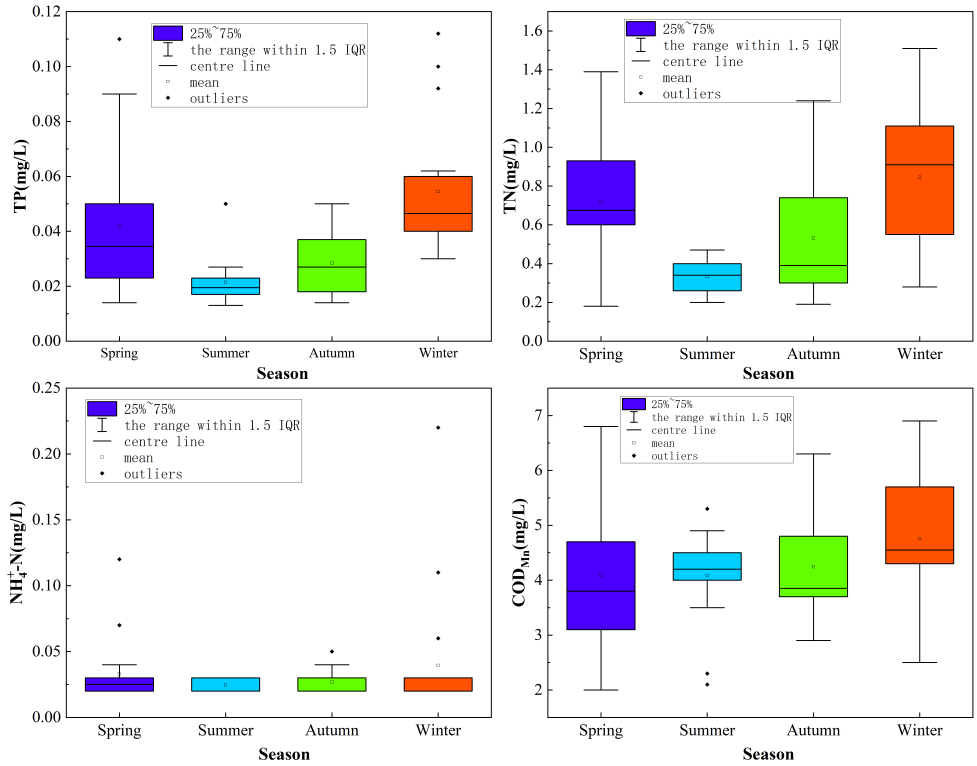


Figure 8. Seasonal variations in water quality indicators in Lake Daguan from 2020 to 2025.

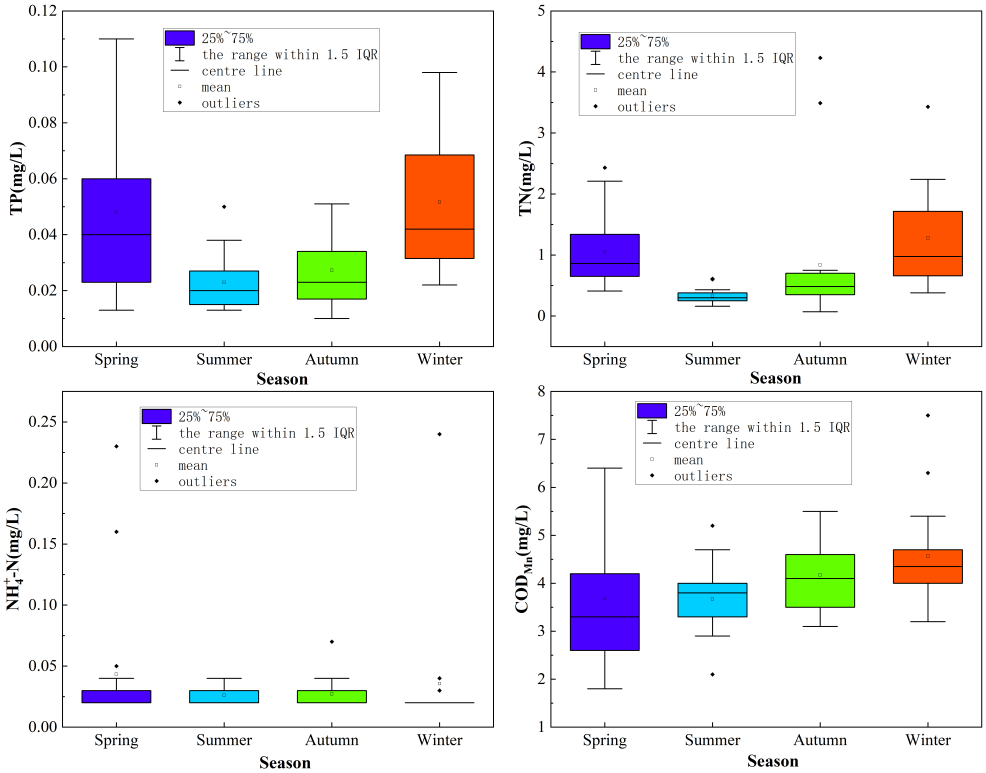


Figure 9. Seasonal variations in water quality indicators in Lake Huang from 2020 to 2025.

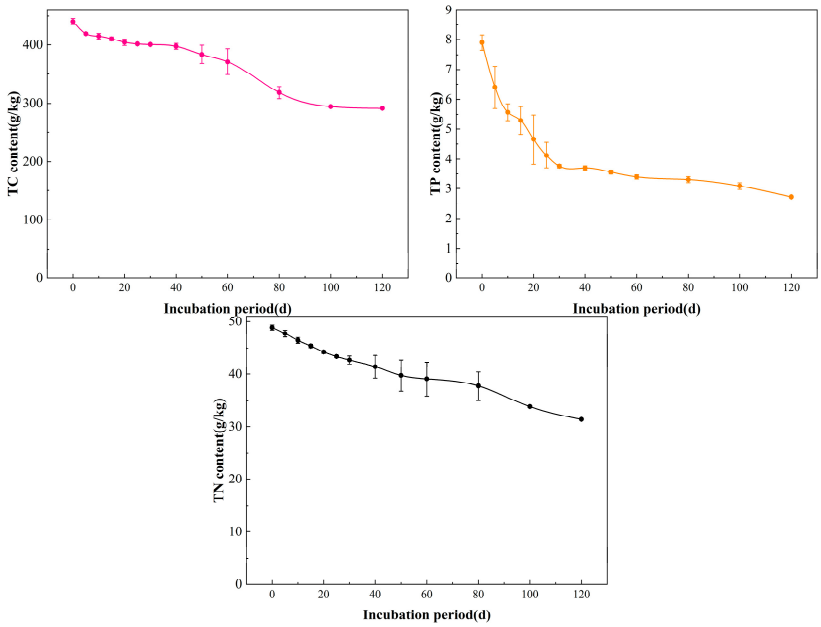


Figure 10. Variations in TC, TN, and TP in decomposing *P. crispus* residues.

4.3. Attenuation Model Analysis

Kinetic models play a pivotal role in quantifying the element release characteristics of plant residues. In this study, the residual rates of each element were fitted using either the asymptotic exponential model or the Olson exponential model, based on the goodness of fit (R^2); the fitting results are summarized in Table 4. The decomposition rate constants derived from these models (TP $\gg$ TN $\approx$ TC) corroborate the aforementioned asynchronous release mechanisms. The asymptotic model revealed that the decomposition constant for the labile fraction of TP was as high as 0.0569 d^{-1}, with a half-life ($t_{0.5}$) of only 12.2 d. This confirms that TP release is predominantly controlled by physical processes during the

initial stage, implying that *P. crispus* can release over 50% of its labile phosphorus into the water column within the first two weeks after senescence [30]. In contrast, the release of TN and TC was extremely slow and highly synchronized. The TN decomposition constant ($k = 0.0035\ d^{-1}$) indirectly reflects the immobilization of nitrogen by microorganisms during metabolism. Furthermore, the TC decomposition constant ($k = 0.0034\ d^{-1}$ with a half-life of 203.8 d) exemplifies the recalcitrance of the lignocellulosic carbon skeleton. Based on these kinetic parameters, the management of internal phosphorus loading from *P. crispus* is highly time-sensitive. It is recommended that management authorities advance the critical window for harvesting operations to within 15 days after plant senescence to effectively remove the bulk of the labile internal phosphorus [31].

Table 4. Index decay model calculation results.

Indicator	Fitting Model	Equation Expression	R^2	Half-Life $t_{0.5}$/d	95% Release Time $t_{0.5}$/d	Ecological Significance
TC	Olson Index Attenuation	$C_t = 437.19 \times e^{-0.0034t}$	0.95	203.8	875	The carbon skeleton undergoes slow, continuous mineralization and decomposition ($k \approx 0.0034$)
TN	Olson Index Attenuation	$N_t = 47.99 \times e^{-0.0035t}$	0.99	198.0	861	Nitrogen is continuously released at a rate comparable to that of carbon ($k \approx 0.0035$)
TP	Asymptotic exponential decay	$P_t = 4.65 \times e^{-0.0569t} + 3.10$	0.98	12.2	52.7	P is the key active element. Its release is extremely rapid ($k \approx 0.057$), 16 times faster than C and N, and ultimately stabilizes at approximately 3.1 g/kg

4.4. Temperature Effect Test

4.4.1. Dynamic Monitoring of Basic Physical and Chemical Indicators

To simplify the presentation of temperature effects, the experimental groups M1 (20 °C), M2 (25 °C), and M3 (30 °C) are hereafter referred to as the low-temperature (LT), medium-temperature (MT), and high-temperature (HT) groups, respectively. The dynamic variations in water column DO and pH under different temperature treatments are illustrated in Figure 11. Overall, the DO concentration was characterized by an initial sharp decline followed by a sustained period of deep hypoxia [32]. During the initial stage (0–4 d), oxygen consumption was significantly accelerated in the high-temperature groups; specifically, the DO in the HT group plummeted from an initial 8.53 mg/L to 0.57 mg/L, causing the water column to rapidly enter a hypoxic state (DO < 2.0 mg/L). In the middle stage (6–30 d), the HT group remained at the lowest levels (0.25–0.50 mg/L), while the LT group exhibited relatively flatter fluctuations (0.47–0.73 mg/L). During the late stage (40–120 d), although minor variations in DO were observed (e.g., approximately 0.58 mg/L in the HT group), considering the standard measurement error of the YSI probe (±0.2 mg/L), no substantial recovery of DO occurred. Instead, the water column remained stable within a severely hypoxic microenvironment [33].

The water pH was primarily governed by the dual effects of organic acid release and ammonification during the decomposition process, with high temperatures significantly amplifying the magnitude of pH fluctuations. In the initial stage (0–4 d), high temperatures accelerated the release of organic components, shifting the acid-base balance toward acidity.

The pH in the HT group dropped from 7.02 to a minimum of 6.52 (a 6.1% decrease), which was notably lower than that in the 25 °C (6.68) and 20 °C (6.83) groups [34]. In the middle stage (6–30 d), organic acid consumption and ammonification became the alternatingly dominant processes. Driven by the high temperature, the HT group exhibited a peak-to-valley difference of 1.29 (ranging from 5.98 to 7.27), far exceeding those of the MT group (1.15, 6.03–7.18) and LT group (0.92, 6.21–7.13) [35]. In the late stage (40–120 d), the production and consumption of acidic and alkaline substances reached a dynamic equilibrium, and pH in all groups returned to the neutral range (30 °C: 6.68–7.33; 25 °C: 6.35–6.96; 20 °C: 6.29–7.17).

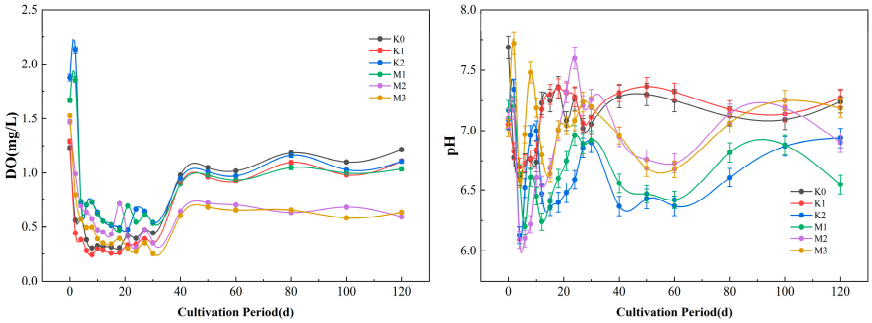


Figure 11. Variations in DO and pH during *P. crispus* decomposition at various temperatures.

4.4.2. Nutrient Release Characteristics

The concentration variations in nutrients released during the decomposition of *P. crispus* at different temperatures are presented in Figure 12. Two-way ANOVA was performed for the entire experimental period, with detailed statistical parameters summarized in Table 5.

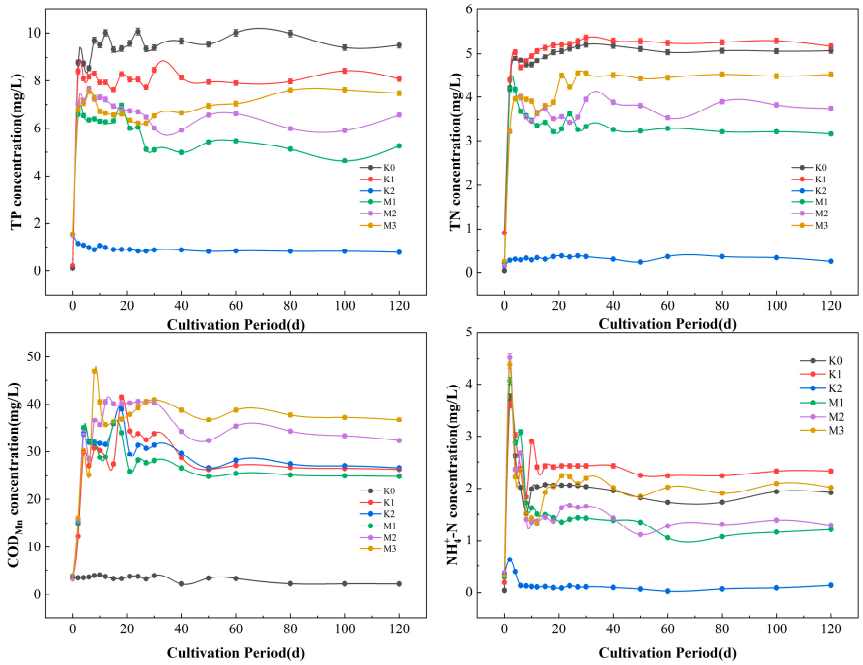


Figure 12. Dynamic variations in water quality parameters during *P. crispus* decomposition at various temperatures (20, 25, and 30 °C). Data are presented as mean ± SD (n = 3).

Table 5. Two-way ANOVA results for the effects of temperature and time on nutrient release.

Source of Variation	Sum of Squares (SS)	Degrees of Freedom (df)	Mean Square (MS)	F-Value	*p*-Value	Partial η^2
TP:Time	43.505	18	2.417	345.28	<0.001 ***	0.982
TP:Temperature	6.923	2	3.462	494.5	<0.001 ***	0.897
TP:Interaction	45.977	36	1.277	182.45	<0.001 ***	0.983
TP:Error	0.798	114	0.007			
TN:Time	14.838	18	0.824	412.16	<0.001 ***	0.985
TN:Temperature	2.499	2	1.25	624.81	<0.001	0.916
TN:Interaction	15.504	36	0.431	215.33	<0.001 ***	0.986
TN:Error	0.228	114	0.002			

Notes: 1. Interaction refers to "Time × Temperature" or "Time × Biomass loading," respectively. 2. *** indicates a highly significant difference at the $p < 0.001$ level. 3. Partial η^2 represents the effect size, indicating that the interaction between time and treatment conditions provides substantial explanatory power for the total data variance.

Time and temperature had a highly significant interaction effect on TP release ($p < 0.001$, Table 5), with high temperatures (25–30 °C) significantly enhancing TP release and maintaining persistently high concentrations compared to 20 °C (Figure 12). At the end of the experiment, the TP concentration in the HT group was 42.1% higher than that in the LT group ($F = 494.5$, $p < 0.001$, Partial $\eta^2 = 0.897$). This effect is driven by two mechanisms: elevated temperatures accelerate plant cell disintegration to promote intracellular phosphate dissolution, and intensify oxygen consumption to form an anaerobic environment, inducing reductive desorption of iron-bound phosphorus from sediment, thereby inhibiting phosphorus sedimentation and fixation [36].

The dynamic variations in the COD_{Mn} responded significantly to temperature, indicating that temperature is the primary driver of organic carbon migration and degradation [37]. In the HT group, COD_{Mn} rose rapidly to a peak of 46.92 mg/L within only 8 days. Conversely, a distinct lag was observed in the LT group, with the peak delayed until day 15 and remaining significantly lower (35.98 mg/L). This initial rapid increase can be attributed to the destruction of plant cell wall structures and the acceleration of solute thermal motion at higher temperatures, leading to an explosive release of soluble organic components [36]. In the late stage (30–120 d), although COD_{Mn} levels declined across all groups due to microbial degradation, the HT group remained at a high level of 36.80 mg/L, significantly higher than the LT group (24.86 mg/L). Contrary to the view that high temperatures favor rapid late-stage organic carbon degradation, our results suggest that while high temperatures enhance heterotrophic microbial metabolic activity, the rate of continuous organic substrate release from the residues far exceeds the microbial mineralization rate in this experimental system [38].

The dynamic evolution of TN concentrations showed marked differentiation under different temperatures. Two-way ANOVA indicated a highly significant interaction between time and temperature ($F = 215.33$, $p < 0.001$, Partial $\eta^2 = 0.986$; Table 5), identifying temperature as the core driver of nitrogen transformation. During the initial stage (0–6 d), TN surged to approximately 4.0 mg/L in all groups (reaching 4.17 mg/L on day 2 in the LT group), primarily due to the rapid physical leaching of soluble nitrogenous components such as proteins [39]. In the middle stage (6–30 d), TN in the HT group continued to rise, reaching 4.54 mg/L on day 27, while the LT group showed a clear decline. This suggests that high temperatures may enhance enzyme activity within the residues, accelerating the enzymatic mineralization of structural organic nitrogen and providing a continuous supply to the water column [32]. In the late stage (30–120 d), TN in the HT group stabilized at a high level of 4.52 mg/L, 42.7% higher than that in the LT group (3.17 mg/L). This contradicts the belief that high temperatures facilitate nitrogen removal. We hypothesize

that in this system, the rate of nitrogen mineralization far exceeds the denitrification rate of the microbial community; furthermore, sustained high oxygen consumption may inhibit ammonia-oxidizing and other nitrifying microorganisms, blocking the conversion of ammonium to nitrate and ultimately leading to the accumulation of soluble nitrogen [40].

The evolution of NH_4^+-N followed a complex pattern of "initial burst—middle recession—late differentiation." In the early stage (0–2 d), driven by the rapid mineralization of easily degradable organic nitrogen, NH_4^+-N quickly peaked (approximately 4.0–4.5 mg/L) before declining rapidly due to the onset of nitrification and microbial assimilation [41]. In the late stage (40–120 d), the 20 °C and 25 °C groups remained stable at low levels (1.2–1.3 mg/L), reflecting a dynamic equilibrium between ammonification and nitrification [42]. However, the HT group exhibited a significant secondary rise, reaching a final concentration of 2.02 mg/L (approximately 1.7 times that of the lower temperature groups). This late-stage differentiation likely results from the impact of high temperature on the coupled ammonification–nitrification metabolism. On one hand, high temperatures may increase deaminase activity, accelerating the decomposition of recalcitrant organic nitrogen; on the other hand, the intensified oxygen consumption under high temperatures creates a persistent hypoxic microenvironment that inhibits aerobic nitrifying bacteria, leading to the retention and accumulation of NH_4^+-N in the water column [43].

4.5. Effect of the Amount Added

4.5.1. Dynamic Physicochemical Indicator Monitoring

The dynamic variations in DO and pH in the water column under different biomass loading treatments are illustrated in Figure 13. The variations in DO concentration were significantly correlated with the biomass loading of *P. crispus*., generally following a three-stage pattern: "initial sharp decline—middle low-level stability—late recovery." Higher biomass loading intensified the initial oxygen consumption. Specifically, the M5 group (40 g) exhibited the fastest oxygen depletion rate during days 0–2. The middle-stage hypoxia (DO < 1 mg/L) in the M5 group persisted for 30 days, which was significantly longer than those in the M4 (30 g, 27 days) and LT (20 g, 24 days) groups [44]. In the late stage, as the proportion of recalcitrant components in the residues increased, the microbial oxygen consumption rate declined, and reoxygenation became the dominant process. Consequently, the DO in all groups gradually recovered and stabilized, with the differences caused by biomass loading progressively diminishing [45]. High biomass loading, by increasing the supply of decomposition substrates, strengthens initial oxygen consumption and prolongs the duration of hypoxia, thereby creating favorable conditions for reductive reactions associated with internal loading.

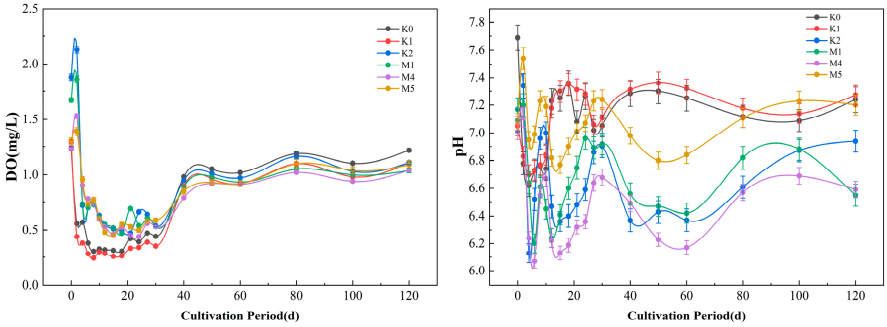


Figure 13. Variations in DO and pH during *P. crispus* decomposition at various addition levels.

The dynamic evolution of pH is essentially the result of a spatiotemporal interplay between "acidogenesis" and "ammonification" during the decomposition process. The initial stage (0–4 d) was the "acid-dominant phase," during which easily degradable

sugars and intracellular substances from *P. crispus* were rapidly leached and converted into small-molecule organic acids (e.g., formic and acetic acids) by fermentative bacteria [7]. This, coupled with the CO_2 produced by respiration, led to a rapid decline in pH to its minimum value. The subsequent middle stage (6–30 d) transitioned into the "ammonification recovery phase." As nitrogenous organic matter (such as proteins) underwent mineralization and decomposition, the intensity of ammonification significantly increased [33]. The resulting alkaline product, NH_4^+-N, consumed protons (H^+) in the water column, creating a buffering effect that prompted the pH to gradually return to a neutral range. Notably, high biomass loading significantly amplified the magnitude of this "acidification-alkalization" fluctuation [46].

4.5.2. Nutrient Release Dynamics

The concentration variations in nutrients released during the decomposition of *P. crispus* under different biomass loadings are presented in Figure 14. Two-way ANOVA was performed for the entire experimental period, with the detailed statistical parameters summarized in Table 6.

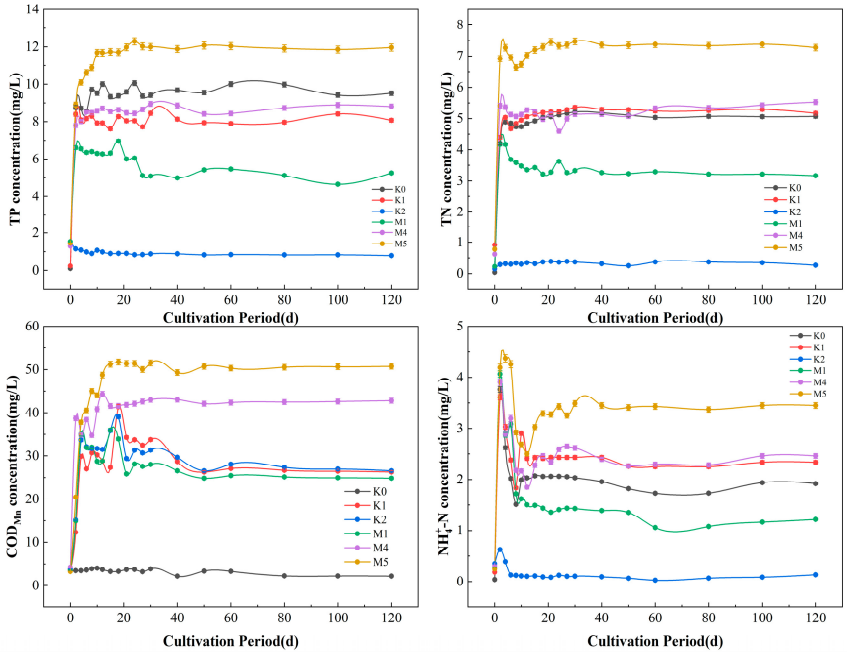


Figure 14. Dynamic variations in water quality parameters during *P. crispus* decomposition at various initial biomass loading levels (20 g, 30 g, and 40 g). Data are presented as mean ± SD (n = 3).

Table 6. Two-way ANOVA results for the effects of biomass loading and time on nutrient release.

Source of Variation	Sum of Squares (SS)	Degrees of Freedom (df)	Mean Square (MS)	F-Value	*p*-Value	Partial η^2
TP:Time	74.292	18	4.127	589.62	<0.001 ***	0.989
TP:Temperature	24.597	2	12.299	1756.93	<0.001 ***	0.969
TP:Interaction	107.899	36	2.997	428.17	<0.001 ***	0.993
TP:Error	0.798	114	0.007			
TN:Time	22.833	18	1.268	634.25	<0.001 ***	0.99
TN:Temperature	8.545	2	4.272	2136.24	<0.001 ***	0.974
TN:Interaction	36.922	36	1.026	512.8	<0.001 ***	0.994
TN:Error	0.228	114	0.002			

Notes: *** indicates a highly significant difference at the $p < 0.001$ level.

As illustrated, the biomass loading of *P. crispus* exerted a significant influence on the dynamic evolution of TP. The initial stage was characterized by differentiated release intensities, while the late stage showed a sustained and stable state of high phosphorus loading. In the high-loading group (40 g, M5), the TP concentration plummeted to a peak of 11.88 mg/L on day 2, which was significantly (1.8 times) higher than that of the low-loading group ($F = 1756.93$, $p < 0.001$, Partial $\eta^2 = 0.969$). The primary driver of this significant discrepancy is the "endogenous phosphorus pool expansion effect" resulting from the difference in initial biomass; an increase in loading directly expands the potential internal phosphorus reservoir in the water column [47]. During the initial stage (0–2 d), rapid tissue rupture of *P. crispus* led to the physical leaching of intracellular water-soluble phosphates [48]. In the late stage (20–120 d), TP in the LT group gradually receded to approximately 5.0 mg/L, whereas the M5 group maintained an extremely high level near 12.0 mg/L without significant attenuation. High biomass loading (40 g) intensifies oxygen demand, maintaining an anaerobic sediment–water interface that triggers reductive dissolution of iron-bound phosphorus (Fe-P) from sediment. This secondary phosphorus release synergizes with continuous plant residue mineralization, leading to persistent high phosphorus concentrations that are difficult to mitigate [49].

The COD_{Mn} concentration exhibited a significant gradient increase with higher biomass loading, confirming that plant residues are the core external contributors to the concentration of oxygen-consuming organic matter. The peak COD_{Mn} concentrations in the high-loading (M5) and medium-loading (M4) groups reached 51.74 mg/L (day 18) and 44.29 mg/L (day 12), respectively—significantly higher than the 35.98 mg/L observed in the LT group. This difference was directly induced by the increase in the total release of organic components from the residues; higher biomass provided a more abundant substrate supply for microbial metabolism, with the release of easily degradable components such as cellulose, hemicellulose, and polysaccharides increasing proportionally with loading [50]. Following the peak, the attenuation rate of COD_{Mn} in the high-loading groups was extremely slow. By the end of the experiment (day 120), the M5 and M4 groups remained at high levels of 50.74 mg/L and 42.79 mg/L, respectively, while the LT group dropped to 24.86 mg/L. This indicates that under high-loading conditions, the microbial degradation process is limited by insufficient dissolved oxygen supply. Excessive organic loading rapidly depletes DO, inhibiting efficient aerobic degradation pathways and forcing microbial metabolism toward low-efficiency anaerobic fermentation [51]. This metabolic shift not only reduces the overall mineralization efficiency of organic pollutants but also significantly extends their retention time in the water column, resulting in prolonged high-concentration organic pollution.

The TN concentration exhibited a significant non-linear dose–response relationship with biomass loading, which was closely linked to a critical threshold. Experimental data showed that in the LT group (20 g), TN remained stable at a lower level of approximately 3.28 mg/L during the middle and late stages (20–120 d), which was significantly lower than the control group average (K0, 5.11 mg/L). This suggests that a moderate addition of *P. crispus* residues (20 g) did not increase the nitrogen load but instead achieved a degree of nitrogen mitigation [28]. Possible reasons include: first, the input of a moderate organic carbon source optimized the water column carbon-to-nitrogen (C/N) ratio, providing a suitable substrate for heterotrophic microbes and promoting their assimilation of inorganic nitrogen into microbial biomass [52]; second, a residue layer of moderate thickness created a physical barrier effect at the sediment–water interface, inhibiting the upward diffusion of endogenous nitrogen from the sediment. However, when the loading increased to 30 g (M4) and 40 g (M5), TN concentrations reached high levels. In the late stage, the TN in the M4 group rose to 5.17 mg/L, approaching control levels, while the M5 group further increased

to 7.37 mg/L. This indicates that when the biomass loading exceeds the critical threshold of 30 g, the flux of nitrogenous organic matter released by excessive decomposition far exceeds the microbial assimilation capacity [7]. Furthermore, the accumulation of excessively thick residues intensifies bottom oxygen consumption. Although hypoxia theoretically favors denitrification, in this high-loading system, the massive nitrogen input rate overwhelmed the natural removal capacity of the system, leading to an exponential increase in TN with loading and a significant nitrogen accumulation effect [53].

The response of NH_4^+-N concentration to biomass loading profoundly reflects the competition and trade-off in microbial metabolic pathways under different substrate loads [54]. The LT treatment group (20 g) maintained an NH_4^+-N concentration of 1.36 mg/L in the middle stage (e.g., day 21), significantly lower than the control (2.06 mg/L), a negative discrepancy that persisted throughout the experiment. Conversely, the M4 and M5 groups consistently stayed above control levels, reaching 2.34 mg/L and 3.27 mg/L on day 21, respectively, showing a clear high-load accumulation effect. Under low loading (20 g), a moderate input of exogenous organic carbon optimized the nutritional structure of the water column, prompting heterotrophic microbes to prioritize the assimilation of inorganic NH_4^+-N into their own biomass (e.g., proteins and nucleic acids), thereby actively reducing the NH_4^+-N concentration [55]. Under high loading (30 g and 40 g), the input of excessive nitrogenous organic matter (such as plant proteins) significantly increased the substrate supply for ammonification, causing the NH_4^+-N generation rate to far exceed microbial demand. Crucially, the massive oxygen consumption during high-biomass decomposition creates a persistent hypoxic environment that severely inhibits the metabolic activity of ammonia-oxidizing and other nitrifying microorganisms, blocking the oxidation of NH_4^+-N to NO_3^--N [56]. The dual effect of an increased generation rate and an obstructed transformation pathway ultimately led to the significant accumulation of NH_4^+-N under high-loading conditions [57].

4.6. Mechanisms Governing Nutrient Release from P. crispus Residues Across Water Matrices

In this study, control groups K1 (deionized water + *P. crispus*) and K2 (lake water + *P. crispus*) exhibited markedly different nutrient dynamic characteristics. While the TN and TP concentrations in the K1 group experienced an explosive increase during the initial stage of the experiment, those in the K2 group remained consistently low; notably, the TP concentration in K2 even showed a downward trend over time (Figure 14). This significant discrepancy primarily stems from the synergistic effects of the physicochemical environment and the microbial community structure [58].

Firstly, the "osmotic shock" effect, caused by the osmotic pressure differential, was the primary driver for the massive nutrient release in the K1 group. The osmotic pressure of the deionized water environment is extremely low. When *P. crispus* residues were submerged in deionized water, the substantial osmotic gradient between the interior and exterior of the cells triggered a rapid influx of water. This resulted in instantaneous cell membrane rupture (osmotic shock), leading to the massive leaching of intracellular soluble organic matter and N/P nutrients within a very short period [59].

Secondly, the differences in biological assimilation and transformation capacity determined the trajectory of the apparent nutrient concentrations in the water column. The K1 group, utilizing deionized water, lacked a functional microbial and phytoplankton community capable of effectively utilizing nutrients, which led to the net accumulation of released elements. In contrast, the K2 group utilized in situ lake water, which was rich in indigenous phytoplankton and microorganisms (e.g., algae and bacteria). Concurrent with the nutrient release from *P. crispus* decomposition, the biological community in the lake water rapidly assimilated and converted these nutrients into biomass. The observed

decline in TP concentration (from 1.53 mg/L to 0.88 mg/L) provides robust evidence for the strong biological uptake or chemical precipitation mechanisms inherent in the lake water system [9].

Furthermore, chemical precipitation and adsorption processes are non-negligible factors. Cations such as Ca^{2+} and Mg^{2+}, which are abundant in lake water, can react with the phosphates released from *P. crispus* to form insoluble precipitates [60]. Additionally, fine suspended particulate matter in the lake water may remove dissolved nutrients from the aqueous phase through adsorption. Since the K2 group did not include sediment (unlike the experimental M groups), the intrinsic physicochemical purification capacity of the water phase was amplified and clearly demonstrated in this control setup.

In summary, K1 represents the "potential maximum capacity" for nutrient release from *P. crispus*, whereas K2 reflects the powerful buffering and purification effects of natural biochemical processes against internal loading within a lake ecosystem.

4.7. Mechanisms of Microbial Community Response to the Decomposition Process

The genus-level classification results in Figure 15 indicate that the microbial community in the *P. crispus* decomposition system was not dominated by a single taxon but rather exhibited significant functional group succession. This successional process was primarily driven by *Vogesella*, UBA3006, and unclassified taxa (Others), which occupied three key ecological niches: "low-temperature rapid growth," "high-temperature steady state," and "high-load degradation," respectively.

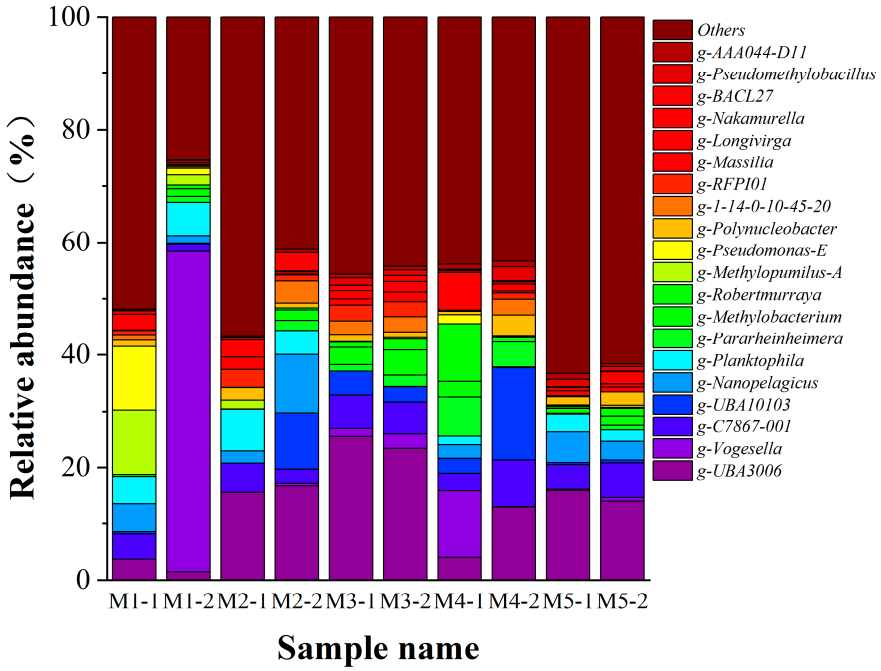


Figure 15. Relative abundance of microbial genera.

Temperature-driven transition from "rapid resource utilization" to "stable symbiosis": At 20 °C (group LT), *Vogesella*, a typical r-strategist, rapidly occupied the ecological niche to utilize labile organic matter. However, its abundance showed substantial intra-group heterogeneity (0.01–56.9%), highlighting the stochasticity inherent in community assembly in low-temperature environments [61]. In contrast, at 30 °C (HT group), high temperatures accelerated the depletion of labile substrates, leading to the rapid exclusion of the fast-growing *Vogesella* (declining to <2%). It was replaced by UBA3006 (stabilizing at 24.4%), which is speculated to possess symbiotic metabolic functions, shifting the micro-ecosystem from disordered resource competition toward an ordered symbiotic network [62].

Biomass-driven succession from "structural dispersion" to "specialized degradation": At a 30 g load (group M4), the co-existence of both easily available and recalcitrant substrates led to intense competition among bacterial groups with different ecological functions. This resulted in a highly dispersed distribution of dominant genera (e.g., UBA10103 and *Vogesella* each accounting for 5–10%), indicating that the community structure was in its most unstable state. When the loading increased to 40 g (group M5), the abundance of recalcitrant substrates and the local hypoxic environment selected for a highly specialized degradation community. The proportion of unclassified taxa (Others, primarily containing Actinobacteria such as Nanopelagicus, which are proficient in lignin degradation) surged to 62.5%. This marks a shift in the core system function toward the decomposition of recalcitrant organic matter, signaling the entry into a stage of deep decomposition. However, it should be noted that these functional successions are inferred from 16S rRNA gene amplicon sequencing taxonomic profiles. Further multi-omics analyses are required to confirm the actual metabolic activities.

5. Conclusions

(1) Temperature is the core driver of *P. crispus* decomposition, and 30 °C significantly amplifies TP release and hypoxia risk in the water column. A biomass loading of 30 g per reactor was identified as the critical threshold for water quality deterioration, beyond which the water self-purification capacity is overwhelmed.

(2) Nutrient release from *P. crispus* residues shows significant asynchrony, with TP release dominated by rapid physical leaching (half-life 12.2 d), while TN and TC release are dependent on slow microbial mineralization, with decomposition rates 16 times lower than TP.

(3) Microbial communities exhibit distinct functional succession during decomposition: low-temperature environments are dominated by r-strategist *Vogesella*, while high temperatures and high biomass loading select for symbiotic and specialized degrading taxa, respectively.

(4) For the management of the Huayang Lakes, it is recommended to harvest *P. crispus* within 15 d after senescence, and implement bottom aeration in high-biomass areas to mitigate anaerobic phosphorus release.

6. Limitations and Future Prospects

While this study systematically elucidates the characteristics of internal nutrient loading driven by *P. crispus* decomposition, and identifies key regulatory factors and critical management thresholds, three non-negligible limitations still exist, which also point out directions for subsequent in-depth research:

First, there is the limitation of scale extrapolation between laboratory microcosms and natural lake ecosystems. The laboratory microcosm system in this study effectively controlled confounding variables to clarify the independent driving mechanisms of temperature and biomass loading, but it cannot fully replicate the complex environmental heterogeneity of natural shallow lakes. Key environmental processes such as wind-wave disturbance, hydrological connectivity, sediment resuspension, and multi-trophic level interactions in the food web were not included in the simulation. Therefore, the critical biomass threshold identified in this study is only applicable to the experimental conditions, and its applicability in field management needs to be further verified and calibrated through in situ mesocosm control experiments and long-term continuous field monitoring in the Huayang Lakes.

Second, there is the limitation of the single-factor experimental design in quantifying interactive effects. This study used a single-factor control design to decouple the inde-

pendent effects of temperature and biomass loading, which is conducive to clarifying the core driving role of each factor. However, in the context of global climate change, the co-occurrence of extreme high temperatures and massive accumulation of macrophyte litter is a common scenario in natural lakes. The current single-factor design cannot fully quantify the synergistic amplification effect of climate warming and high biomass accumulation on nutrient release and eutrophication risk, which may lead to an underestimation of the actual ecological risk in field conditions. To fill this gap, subsequent studies will establish a full factorial experimental matrix with full-gradient cross-combinations of temperature and biomass loading to systematically explore the interactive effects of the two factors and improve the accuracy of the eutrophication risk prediction model.

Third, there is the insufficient depth of the microbial driving mechanism analysis. This study only revealed the succession pattern of the bacterial community during *P. crispus* decomposition based on 16S rRNA gene sequencing, which can only reflect the composition of the microbial community, but cannot clarify the functional gene expression, metabolic activity, and key regulatory pathways of core degrading flora. In subsequent studies, we will integrate multi-omics techniques (metagenomics and metatranscriptomics) and extracellular enzyme activity assays to systematically analyze the microbial driving mechanism of nutrient cycling on the "gene-enzyme-substrate" level and provide a more solid theoretical basis for the precise regulation of internal loading in shallow lakes.

Author Contributions: Data Collection: X.J., Y.Y. and H.X. Field Sampling: X.J., L.Z., Y.Y. and N.L. Data Processing: Y.Y. Laboratory Simulation: X.J., Z.L., H.X. and N.L. Experimental Analysis: X.J. Text Revision: F.M. and Z.L. All authors have read and agreed to the published version of the manuscript.

Funding: This research received no external funding.

Data Availability Statement: The original contributions presented in this study are included in the article. Further inquiries can be directed to the corresponding author.

Acknowledgments: The authors would like to express their gratitude to the staff of the Huayang Lakes Management Bureau for their assistance in field sampling and data collection. We also thank Water Pollution Control Simulation Laboratory for providing the use of the elemental analyzer. During the preparation of this manuscript, the author(s) used deepL (Version 4.5) for the purposes of refining the language, improving the clarity of the text, and assisting in the structuring of the initial draft based on experimental data. The authors have reviewed and edited the output and take full responsibility for the content of this publication.

Conflicts of Interest: The authors declare no conflicts of interest.

References

1. Lv, C.; Tian, Y.; Huang, L.; Shan, H.; Chou, Q.; Zhang, W.; Su, H.; Li, K.; Zhang, X.; Ni, L.; et al. Buffering capacity of submerged macrophytes against nutrient pulses increase with its coverage in shallow lakes. *Chemosphere* **2023**, *332*, 138899. [CrossRef]
2. Zhang, X.; Zhang, J.; Li, Z.; Wang, G.; Liu, Y.; Wang, H.; Xie, J. Optimal submerged macrophyte coverage for improving water quality in a temperate lake in China. *Ecol. Eng.* **2021**, *162*, 106177. [CrossRef]
3. Zhang, C.; Li, Q.; Zhang, L.; Zhang, J. Responses of submerged macrophytes *Vallisneria natans* and epiphytic biofilm to floating plants *Eichhornia crassipes* in eutrophic water. *Water Environ. Res.* **2021**, *93*, 2237–2249. [CrossRef]
4. Wang, D.; Gan, X.; Wang, Z.; Jiang, S.; Zheng, X.; Zhao, M.; Zhang, Y.; Fan, C.; Wu, S.; Du, L. Research status on remediation of eutrophic water by submerged macrophytes: A review. *Process Saf. Environ. Prot.* **2023**, *169*, 671–684. [CrossRef]
5. Chen, H.; Zhang, S.; Lv, X.; Guo, S.; Ma, Y.; Han, B.; Hu, X. Interactions between suspended sediments and submerged macrophytes-epiphytic biofilms under water flow in shallow lakes. *Water Res.* **2022**, *222*, 118911. [CrossRef]
6. Wang, L.; Zhang, L.; Song, H.; Dong, B.; Wang, Y.; Yu, W.; Wu, Y.; Wu, X.; Ge, X. The Effect of the *Potamogeton crispus* on Phosphorus Changes throughout Growth and Decomposition: A Comparison of Indoor and Outdoor Studies. *Sustainability* **2023**, *15*, 3372. [CrossRef]

7. Shi, P.; Wang, H.; Feng, M.; Cheng, H.; Yang, Q.; Yan, Y.; Xu, J.; Zhang, M. Bacterial Metabolic Potential in Response to Climate Warming Alters the Decomposition Process of Aquatic Plant Litter—In Shallow Lake Mesocosms. *Microorganisms* **2022**, *10*, 1327. [CrossRef]
8. Yan, D.; Zhang, X.; Zhang, Z.; Cao, X.; Ma, J.; Zhang, Y.; Zhang, W. Decay Dynamics of Hydrophyte and Nutrient Release in a Lake System: Experimental and Predicting Modeling. *ACS ES&T Water* **2024**, *4*, 4943–4957. [CrossRef]
9. Bao, S.; Jin, L.; Wu, Q.; Xie, S.; Xu, J.; Peng, S.; Liu, C.; Pan, Y. Effects of Interspecific Interactions on Aquatic Macrophyte Litter Decomposition and Its Influencing Factors. *ACS ES&T Water* **2023**, *3*, 3755–3766. [CrossRef]
10. Evans, L.C.; Melero, Y.; Schmucki, R.; Boersch-Supan, P.H.; Brotons, L.; Fontaine, C.; Jiguet, F.; Kuussaari, M.; Massimino, D.; Robinson, R.A.; et al. Mechanisms underpinning community stability along a latitudinal gradient: Insights from a niche-based approach. *Glob. Change Biol.* **2023**, *29*, 3271–3284. [CrossRef] [PubMed]
11. Wang, Y.; Fan, Z.; Wang, W.; Zhou, Z.; Ye, X. Effects of Flood on Phytoplankton Diversity and Community Structure in Floodplain Lakes Connected to the Yangtze River. *Diversity* **2022**, *14*, 581. [CrossRef]
12. An, L.; Liu, C.; Fan, Z.; Liao, K.; Wang, W.; Wang, N. Effects of water level variations on the water quality of Huayang Lakes, China. *J. Geogr. Sci.* **2025**, *35*, 173–188. [CrossRef]
13. Cheng, Q.; Li, L.; Dong, X.; Li, Y.; Kattel, G. Plant Macrofossils Reveal Aquatic Macrophyte Successions of a Typical Shallow Lake (Huanggai Lake, China) in the Past Century. *Plants* **2022**, *11*, 1413. [CrossRef] [PubMed]
14. Yang, K.; Yin, Y.; Xu, Y.; Wang, S.; Gao, M.; Peng, K.; Luo, J.; Gao, J.; Cai, Y. Hydrometeorological conditions drive long-term changes in the spatial distribution of *Potamogeton crispus* in a subtropical lake. *Front. Plant Sci.* **2024**, *15*, 1424300. [CrossRef]
15. Liu, Y.; Wu, T.; Wang, S.; Xia, K.; Wang, X.; Du, P. A phenomenology-based algorithm for extracting submerged aquatic vegetation in lakes using Sentinel-2 time seriesImagery: A case study of *Potamogeton crispus*. *GIScience Remote Sens.* **2025**, *62*, 2479969. [CrossRef]
16. Hou, X.; Liu, J.; Huang, H.; Zhang, Y.; Liu, C.; Gong, P. Mapping global lake aquatic vegetation dynamics using 10-m resolution satellite observations. *Sci. Bull.* **2024**, *69*, 3115–3126. [CrossRef]
17. Li, X.; Cui, B.; Yang, Q.; Lan, Y.; Wang, T.; Han, Z. Effects of plant species on macrophyte decomposition under three nutrient conditions in a eutrophic shallow lake, North China. *Ecol. Model.* **2013**, *252*, 121–128. [CrossRef]
18. *HJ 636-2012*; Water Quality-Determination of Total Nitrogen-Alkaline Potassium Persulfate Digestion UV Spectrophotometric Method. China Environmental Science Press: Beijing, China, 2012.
19. *GB 11893-89*; Water Quality-Determination of Total Phosphorus-Ammonium Molybdate Spectrophotometric Method. Standards Press of China: Beijing, China, 1989.
20. *GB 11892-89*; Water Quality-Determination of Permanganate Index. Standards Press of China: Beijing, China, 1989.
21. *HJ 535-2009*; Water Quality-Determination of Ammonia Nitrogen-Nessler's Reagent Spectrophotometric Method. China Environmental Science Press: Beijing, China, 2009; 21.
22. Hrustić, E.; Bobanović-Ćolić, S. Hypoxia in deep waters of moderately eutrophic marine lakes, Island of Mljet, eastern Adriatic Sea. *Sci. Mar.* **2017**, *81*, 431–447. [CrossRef]
23. Bai, X.; Jiang, Z.; Fang, Y.; Zhu, L.; Feng, J. Effects of Environmental Concentrations of Total Phosphorus on the Plankton Community Structure and Function in a Microcosm Study. *Int. J. Environ. Res. Public Health* **2022**, *19*, 8412. [CrossRef]
24. Qin, B.; Zhou, J.; Elser, J.J.; Gardner, W.S.; Deng, J.; Brookes, J.D. Water Depth Underpins the Relative Roles and Fates of Nitrogen and Phosphorus in Lakes. *Environ. Sci. Technol.* **2020**, *54*, 3191–3198. [CrossRef] [PubMed]
25. Yin, J.; Chen, H.; Wang, Y.; Guo, L.; Li, G.; Wang, P. Ammonium Nitrogen Streamflow Transport Modelling and Spatial Analysis in Two Chinese Basins. *Water* **2022**, *14*, 209. [CrossRef]
26. Ferreira, T.F.; Crossetti, L.O.; Marques, D.M.L.M.; Cardoso, L.; Fragoso, C.R.; Nes, E.H.v. The structuring role of submerged macrophytes in a large subtropical shallow lake: Clear effects on water chemistry and phytoplankton structure community along a vegetated-pelagic gradient. *Limnologica* **2018**, *69*, 142–154. [CrossRef]
27. Wei, Y.; Zhang, M.; Cui, L.; Pan, X.; Liu, W.; Li, W.; Lei, Y. Winter Decomposition of Emergent Macrophytes Affects Water Quality under Ice in a Temperate Shallow Lake. *Water* **2020**, *12*, 2640. [CrossRef]
28. Li, X.; Lun, X.; Niu, J.; Zhang, L.; Wu, B.; Wang, X. Remediation Effects of *Potamogeton crispus* on Nitrogen-Loaded Water Bodies and Its Greenhouse Gas Emission Mechanisms. *Atmosphere* **2025**, *16*, 803. [CrossRef]
29. Lei, J.; Zhang, S.; Chen, H.; Li, Y.; Yuan, W.; Qu, A. Mechanisms of carbon sequestration via interactions between dissolved organic matter (DOM) and bacteria during floating-leaf macrophyte decline. *Carbon Res.* **2026**, *5*, 24. [CrossRef]
30. Wang, H.; Zhang, R.; Chen, Q.; Chen, K.; Hu, R. Interspecific Differences in the Effects of Calcium and Phosphorus Coprecipitation Induced by Submerged Plants on the Water-to-Phosphorus Cycle. *Sustainability* **2024**, *16*, 4200.
31. Li, H.; Deng, H.; Li, J.; Qin, Z.; Chen, F.; Duan, X. The impact of the unharvested reeds on the nitrogen and phosphorus cycles in Lake Dongting. *J. Freshw. Ecol.* **2025**, *40*, 2557554. [CrossRef]
32. Wang, H.; Cui, Y.; Ma, J.; Pei, Z.; Bian, G.; He, F.; Ji, M.; Xu, X. Decomposition of cyanobacteria and submerged macrophytes: Impacts on carbon emissions and nutrient cycling in lake ecosystems. *Carbon Res.* **2026**, *5*, 18. [CrossRef]

33. Cao, D.; Li, N.; Yang, Y.; Wang, D. Seasonal Variation Affects Aquatic Macrophyte Litter Decomposition and Invertebrate Colonization in a Subtropical Eutrophic Shallow lake, China. *Wetlands* **2025**, *45*, 14. [CrossRef]
34. Cao, H.; Zhang, C.; Yang, B.; Liu, L.; Wang, J.; Zheng, X. Synergistic Remediation of Eutrophic Rural Pond Water Using Submerged Macrophytes and Daphnia magna. *Plants* **2025**, *14*, 3136. [CrossRef]
35. Ning, Y.; Gao, B.; Wang, H.; Hou, W. Effects of pH, temperature and hydraulic disturbance on nitrogen release from sediments in the Sunxi River, Three Gorges Reservoir Area, China. *PeerJ* **2025**, *13*, e19161. [CrossRef] [PubMed]
36. Li, Q.; Zhang, R.; Yuan, H.; Wang, L.; Xu, S. Unraveling the Molecular Composition and Reactivity Differentiation of Algae- and Macrophyte-Derived Dissolved Organic Matter in Plateau Lakes: Insights from Optical Properties and High Resolution Mass Spectrometry Characterization. *Molecules* **2025**, *30*, 3510. [CrossRef]
37. Zhu, D.; Hang, X.; Xu, M.; You, X.; Wang, X.; Zhou, L.; Wang, Y. Interactions between iron and sulfur on the release and dynamics of phosphorus in eutrophic lake sediments. *J. Soils Sediments* **2024**, *25*, 313–327. [CrossRef]
38. Li, Z.; Xu, Z.; Yang, Y.; Stewart, R.I.A.; Urrutia-Cordero, P.; He, L.; Zhang, H.; Hansson, L.-A. Heat Waves Alter Macrophyte-Derived Detrital Nutrients Release under Future Climate Warming Scenarios. *Environ. Sci. Technol.* **2021**, *55*, 5272–5281. [CrossRef]
39. Hu, L.; Xiao, L.; Wang, T. Dynamics of Nitrogen and Phosphorus Release from Submerged Soil–Plant Systems in the Three Gorges Reservoir. *Water* **2025**, *17*, 1701. [CrossRef]
40. Zhang, L.; Bai, J.; Zhai, Y.; Zhang, K.; Wang, Y.; Tang, R.; Xiao, R.; Jorquera, M.A. Seasonal changes in N-cycling functional genes in sediments and their influencing factors in a typical eutrophic shallow lake, China. *Front. Microbiol.* **2024**, *15*, 1363775. [CrossRef]
41. Wei, C.; Zhang, W. Nitrogen Contribution Rate of Anammox in Different Systems and Its Relationship with Environmental Factors. *Water* **2023**, *15*, 2101. [CrossRef]
42. Bauduin, T.; Gypens, N.; Borges, A.V. Methane, carbon dioxide, and nitrous oxide emissions from two clear-water and two turbid-water urban ponds in Brussels (Belgium). *Biogeosciences* **2025**, *22*, 3785–3805. [CrossRef]
43. Tang, W.; Fortin, S.G.; Intrator, N.; Lee, J.A.; Kunes, M.A.; Jayakumar, A.; Haynes, S.J.; Oleynik, S.; Sigman, D.M.; Ward, B.B. Similar Oxygen Sensitivities of Different Steps of Denitrification in Estuarine Waters. *Environ. Sci. Technol.* **2025**, *59*, 7165–7175. [CrossRef]
44. Hu, W.; Wei, W.; Ye, C.; Li, C.; Zheng, Y.; Shi, X.; Chen, H. Determining the Optimal Biomass of Macrophytes during the Ecological Restoration Process of Eutrophic Shallow Lakes. *Water* **2021**, *13*, 3142. [CrossRef]
45. Panhota, R.S.; da Cunha Santino, M.B.; Bianchini, I., Jr. Oxygen consumption and formation of recalcitrant organic carbon from the decomposition of free-floating macrophyte leachates. *Environ. Sci. Pollut. Res. Int.* **2023**, *30*, 101379–101391. [CrossRef]
46. Deng, H.; Zhang, J.; Wu, J.; Yang, L.; Zhang, Y.; Yao, X. Physicochemical properties and greenhouse gas emissions of water body during the decomposition of *Potamogeton crispus* with different values of initial debris biomass. *Environ. Sci. Pollut. Res. Int.* **2021**, *29*, 5505–5516. [CrossRef] [PubMed]
47. Zhao, S.; Hermans, M.; Niemistö, J.; Jilbert, T. Elevated internal phosphorus loading from shallow areas of eutrophic boreal lakes: Insights from porewater geochemistry. *Sci. Total Environ.* **2023**, *907*, 167950. [CrossRef] [PubMed]
48. Zhang, K.; Li, T.; Chai, Y.; Dai, B.; Pan, Q.; Wu, J.; Zhou, Q.; Zhao, L.; Huang, Y. Internal Cycling Influences Nutrient Changes Leading to Altered Nutrient Limitation in Eutrophic Lake. *Water* **2025**, *17*, 2604. [CrossRef]
49. Tao, Y.; Ma, S.; Cao, M.; Li, J.; Wang, F.; Gao, Z.; Xu, Q.; Guo, J.; Sun, K.; Wang, F. Recent advances on iron bound phosphorus in wetland sediments: Characteristics, influencing factors, interactions with organic matter and emerging contaminants. *Environ. Pollut.* **2025**, *383*, 126826. [CrossRef]
50. Chen, P.; Mei, T.; He, X.; Lin, Y.; He, Z.; Kong, X. Impacts of Lead and Nanoplastic Co-Exposure on Decomposition, Microbial Diversity, and Community Assembly Mechanisms in Karst Riverine Miscanthus Litter. *Microorganisms* **2025**, *13*, 2172. [CrossRef]
51. Chinedu Agu, P.C.; Ezeh, E.M.; Aworabhi, E. Biological Treatment Techniques for Sewage: Aerobic and Anaerobic Processes. In *Sewage-Management and Treatment Techniques*; Abu Hasan, H., Ed.; IntechOpen: London, UK, 2024.
52. Velthuis, M.; Zoccarato, L.; Veraart, A.J.; Monaghan, M.T.; Funke, E.; Verdonschot, P.; Grossart, H.-P.; Hilt, S. Light-Driven Changes in Macrophyte Tissue Quality Affect the Composition of Associated Microbial Communities. *Microb. Ecol.* **2025**, *88*, 52. [CrossRef]
53. Huang, Y.; An, S. Weak Hypoxia Enhanced Denitrification in a Dissimilatory Nitrate Reduction to Ammonium (DNRA)-Dominated Shallow and Eutrophic Coastal Waterbody, Jinhae Bay, South Korea. *Front. Mar. Sci.* **2022**, *9*, 897474. [CrossRef]
54. Li, L.; Zhao, D.; Du, R.; Tang, K.; Zhang, Y. Niche adaptation of particle-associated ammonia-oxidizing archaea sustains nitrification under marine deoxygenation. *Front. Microbiol.* **2026**, *17*, 1773718. [CrossRef]
55. Chen, S.; Sun, X.; Tian, X.; Jiang, W.; Dong, X.; Li, L. Influence of ammonia nitrogen management strategies on microbial communities in biofloc-based aquaculture systems. *Sci. Total Environ.* **2023**, *903*, 166159. [CrossRef] [PubMed]
56. Sun, J.; Yang, X.; Yu, L.; Zhang, Q.; Yung, C.C.M.; Li, J. Hypoxia Decreases Nitrogen Removal in Coastal Marine Sediments. *Environ. Sci. Technol.* **2026**, *60*, 10763–10774. [CrossRef]

57. Lv, C.; Shi, L.; Tian, Y.; Shan, H.; Chou, Q.; Liu, W.; Li, K.; Cao, T. Quantifying Critical Thresholds of Submerged Macrophyte Coverage to Buffer Climate-Amplified Ammonium Pulses and Stabilize Clear-water States. *Environ. Sci. Technol.* **2025**, *59*, 17070–17083. [CrossRef]
58. Mijanur, R.M.; Nushin, H.; Hamid, H. Recovering Microalgal Bioresources: A Review of Cell Disruption Methods and Extraction Technologies. *Molecules* **2022**, *27*, 2786. [CrossRef] [PubMed]
59. Li, Z.; Wang, H.; Zhou, Y.; Wang, M. Calcium–phosphorus coprecipitation induced by *Hydrilla verticillata* photosynthesis: Response to elevated phosphorus concentration and regulation by light intensity, inorganic carbon and calcium levels. *J. Freshw. Ecol.* **2025**, *40*, 2603114. [CrossRef]
60. Babcock, M.; Romanelli, K.; Gonzalez, S.; Robinson, G.; Newell, P.D. Regulation of indigoidine production in *Vogesella indigofera* by a novel two-component system. *J. Bacteriol.* **2025**, *208*, e0036425. [CrossRef]
61. Liu, J.; Huang, X.; Jiang, X.; Qing, C.; Li, Y.; Xia, P. Loss of submerged macrophytes in shallow lakes alters bacterial and archaeal community structures, and reduces their co-occurrence networks connectivity and complexity. *Front. Microbiol.* **2024**, *15*, 1380805. [CrossRef] [PubMed]
62. Zhou, Z.; Tran, P.Q.; Martin, C.; Rohwer, R.R.; Baker, B.J.; McMahon, K.D.; Anantharaman, K. A 20-year time-series of a freshwater lake reveals seasonal dynamics and environmental drivers of viral diversity, ecology, and evolution. *bioRxiv* **2024**. [CrossRef]

Disclaimer/Publisher's Note: The statements, opinions and data contained in all publications are solely those of the individual author(s) and contributor(s) and not of MDPI and/or the editor(s). MDPI and/or the editor(s) disclaim responsibility for any injury to people or property resulting from any ideas, methods, instructions or products referred to in the content.